Journal of
Ceramic Science
and Technology

J. Ceram. Sci. Tech., 02 [04] 217-226 (2011)
DOI: 10.4416/JCST2011-00038
available online at: http://www.ceramic-science.com

Feasibility Study on Rapid Prototyping of Porcelain Products

X. Tian[1], T. Mühler[2], C. Gomes[3], J. Günster[*3], J.G. Heinrich[2]

[1]State Key Laboratory of Mechanical Manufacture
System Engineering, Xi'an Jiaotong University, Xi'an 710049, China
[2]Department for Engineering Ceramics, Clausthal University of
Technology, 38678 Clausthal-Zellerfeld, Germany
[3]BAM Federal Institute of Materials Research and Testing, Berlin, Germany

received September 27, 2011; received in revised form November 10, 2011; accepted November 18, 2011

Abstract

In order to reduce the time to market of new or customized porcelain products or artworks, rapid prototyping using layer-wise slurry deposition (LSD) was studied in the present research. The properties such as phase composition, microstructure, shrinkage, density, and mechanical strength, of laser-sintered (LS) and biscuit-fired (BF) samples before and after post-sintering in a furnace were studied and compared with each other. The laser-sintered sample was comparable with the biscuit-fired sample with regard to porosity, but had just half the mechanical strength of the latter. The feasibility of rapid prototyping of porcelain products was validated by the successful fabrication of two models (thick-wall pipe and double heart), which showed that the relatively low mechanical strength of the laser-sintered samples was still high enough for the downstream handling processes.

Keywords: Layer-wise slurry deposition, mechanical properties, porcelain, structural applications, rapid prototyping

I. Introduction

The general purpose of rapid prototyping is to reduce the time to market for new products by shortening the period between design and testing. The prototypes or parts are designed with computer-aided design (CAD) software and fabricated in a rapid manufacturing unit without any requirements for dedicated tooling. When rapid prototyping processes, such as stereolithography (SL) [1] selective laser sintering [2] and fused deposition modeling [3], appeared twenty years ago, their primary aim was the production of prototypes using polymers as the raw material. Metallic materials were then used in the rapid prototyping processes to produce selected functional parts in low quantities by means of selective laser sintering of metallic powder [4], direct metal deposition [5], etc. After polymer and metallic materials, ceramics were employed in the solid freeform fabrication processes to produce selected components with complex structures that could not be fabricated with conventional methods. Ceramic-powder-loaded light-sensitive resins were used in the SL process [6]. Fused deposition and extrusion processes utilized ceramic-loaded filaments or paste to produce ceramic green parts [7, 8]. The parts prepared with all these processes need post-treatment in a furnace to remove the organic additives. The final ceramic parts always have relatively low bulk density and mechanical strength. So, ceramic powders without any organic additives were sintered by means of lasers to improve the density and mechanical strength of the ceramic components produced [9, 10]. Owing to the difficulty in preparing a dense powder matrix, which has a significant influence on the density of the laser-sintered bodies, the layer-wise slurry deposition (LSD) process has been developed [11, 12, 13] and used in the present research. There are two advantages when using water-based binder-free ceramic slurries as the starting materials. First, layer-wise-deposited slurry achieves a relatively high green density of the dried ceramic film before laser sintering. The laser sintering is therefore more activated and the density of laser-sintered bodies can be improved. Second, the ceramic slurry from the conventional porcelain manufacturing processes can be directly used in the LSD process. The proposal of rapid prototyping of porcelain products is based on this consideration for the LSD process. Prototypes of the porcelain products are required for evaluation before introducing a new or customized design into the market. The ability to deliver such prototypes in a reasonable time and at an acceptable price can be a decisive factor in a competitive market. However, conventional ceramic fabrication processes have the disadvantage that they are normally suitable for mass production instead of fast and economical manufacturing of prototypes or small-scale series. Porcelain slurry especially for the conventional slip casting process can be taken from ceramic factories and directly used in the present LSD process to produce prototypes of a new design. The cost and lead time for the prototypes can be reduced drastically because there is no need for moulds, which are always used in conventional processes. Certainly, customized ceramic artworks with complex designs can also be produced with this LSD process.

* Corresponding author: jens.guenster@bam.de

The common procedure for sintering porcelain ceramics is to fire the ware initially to a low temperature (biscuit firing, BF), then to apply the glaze and fire it again at a higher temperature (glost firing, GF) [14]. In the present research, the properties of biscuit-fired (BF) and laser-sintered (LS) porcelain bodies were studied and compared. If the properties of LS samples are comparable with those of the BF samples, LS bodies can be used to substitute the latter and glost-fired. Finally, porcelain prototypes of a new design can be produced in a very short time with a low manufacturing cost.

II. Experimental Procedure

(1) Starting Materials and Characterization

In the present research, the properties of the LS samples were compared with those of the BF samples before and after post-sintering. The LS samples were prepared with the LSD-based direct laser sintering process with the following process parameters: laser power of 20 W, scan speed of 100 mm/s, hatch spacing of 0.1 mm, and layer thickness of 0.1 mm. The biscuit-fired samples were slip cast using the same commercially available porcelain slurry and then biscuit-fired in a furnace at 900 °C. The solid content of this slurry is around 87 wt%. The average particle size of the slurry is 8.317 μm. Chemical and phase compositions of the green body, and the biscuit-fired, laser-sintered and glost-fired porcelain bodies were identified by means of X-ray diffraction (Siemens diffractometer D 5000, Siemens AG, Germany). TG/DT analyses of the dried slurry, laser-sintered and biscuit-fired bodies were conducted with a Netzsch STA 409 analyzer (Germany). Density and porosity of all the specimens were measured using a Pycnomatic ATC and Pascal 240 mercury intrusion porosimeter (Thermo Electron Corporation, Italy). Shrinkage of the samples during the glost-firing process was measured with a dilatometer on samples measuring 10 mm in length. Four-point bending strength was measured according to DIN/EN 843, part 1, with a sample geometry of 3 x 4 x 45 mm, an outer span of 40 mm and an inner span of 20 mm. There were four specimens for each measurement group. The LS specimens for the bending strength test were fabricated in a size measuring 45 mm × 4 mm × 3 mm. The BF specimens were cut from biscuit-fired porcelain blocks. The surfaces of the two samples were not polished, as new surface defects will appear during the surface polishing process owing to the layered and porous microstructure of the samples. The force was loaded on the laser-sintered surface of LS samples. The microstructures of all samples were studied with scanning electron microscopy (SEM, CamScan CS4 Cambridge, UK), on fractured and etched cross-sections of the specimens.

(2) Layer-Wise Slurry Deposition

The LSD-based laser sintering process for the ceramic components is shown in Fig. 1. A worktable with a high kinematic resolution, 1 μm/step for vertical (lowering of the part for each layer) and horizontal motion (deposition of the slurry), is used to achieve the slurry multilayer deposition process. Similar to the tape-casting process the slurry is supplied by a dispenser pump (Dispenser 3NDP8, Netzsch, Germany) and deposited via a doctor blade on a preheated (up to 200 °C) tile. A 100 W IPG single mode YAG-fiber laser system (wave length 1.064 m, Burbach, Germany) and a galvano-scanner (Hurryscan, Scanlab AG, Germany) are used to sinter the dried ceramic tape. The focused laser beam has a spot size of 50 μm. The scanner is controlled by software in which the geometry model is sliced into many layers along the direction of fabrication and each layer is hatched in the respective cross-section according to the preset parameters. Repeating the deposition and laser sintering process builds up the final components. The whole part is dipped into water to remove any unsintered ceramic powder. After cleaning, the laser-sintered ceramic parts can be post-sintered in a furnace if necessary. In the present research, all the experiments were conducted on a fully automatic rapid prototyping machine, in which all the fabrication processes are integrated. This machine (LSD 100) was jointly developed by CIC (Ceramic Institute Clausthal GmbH, Clausthal-Zellerfeld, Germany) and T&T (Tools and Technologies GmbH, Schönwald, Germany).

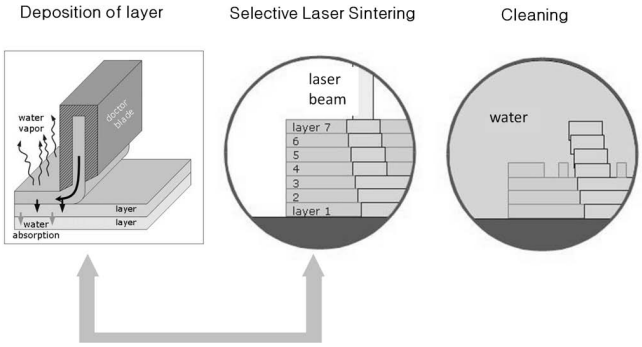

Fig. 1 Schematic of rapid prototyping process using layer-wise slurry deposition [12].

III. Results and Discussion

(1) Laser-Sintered (LS) and Biscuit-Fired (BF) Samples

(a) *Microstructure*

The microstructures of fracture cross-sections in the green body, biscuit-fired, and laser-sintered samples are shown in Fig. 2. The green body was prepared by slip casting, which is a conventional manufacturing process for porcelain products. The plate-like morphology of kaolinite particles is the dominant character of the microstructure in the green body, as shown in Fig. 2a. The basic reactions triggered by the biscuit firing under 900 °C are the dehydroxylation and the α-to β-quartz transformation at 573 °C as well as the removal of water and organics [15, 16, 17]. The microstructure of a 900 °C biscuit-fired sample is shown in Fig. 2b. In this figure, quartz particles are observed surrounded by the porous microstructure. This porous, flake material is metakaolin phase transformed from the dehydroxylation of kaolinite. And metakaolin has structural continuity with the parent material [18, 19]. The microstructure of the fracture cross-section in the laser-sintered sample is shown in Figs. 2c and d. A layer-wise stacked microstructure, ow-

ing to the LSD process in the fracture cross-section, is observed in Fig. 2c. Glass phase and pores are distributed in the two distinct regions: the upper and bottom parts of one single layer, respectively. Glass phase was produced as a result of the high heating and cooling rates in the laser sintering process. The residual quartz particles were trapped in the glass phase, as shown in Fig. 2d. Pores formed when gas bubbles were trapped in the solidifying interface. Gas exists in the deposited single layer and the interface between two adjacent layers in the LSD process. The chemical reactions in the laser sintering process also produce some gases. All these gases are released when the material is melting and form the bubbles or pores in the liquid-solid interface, which is always observed at the bottom of one single layer.

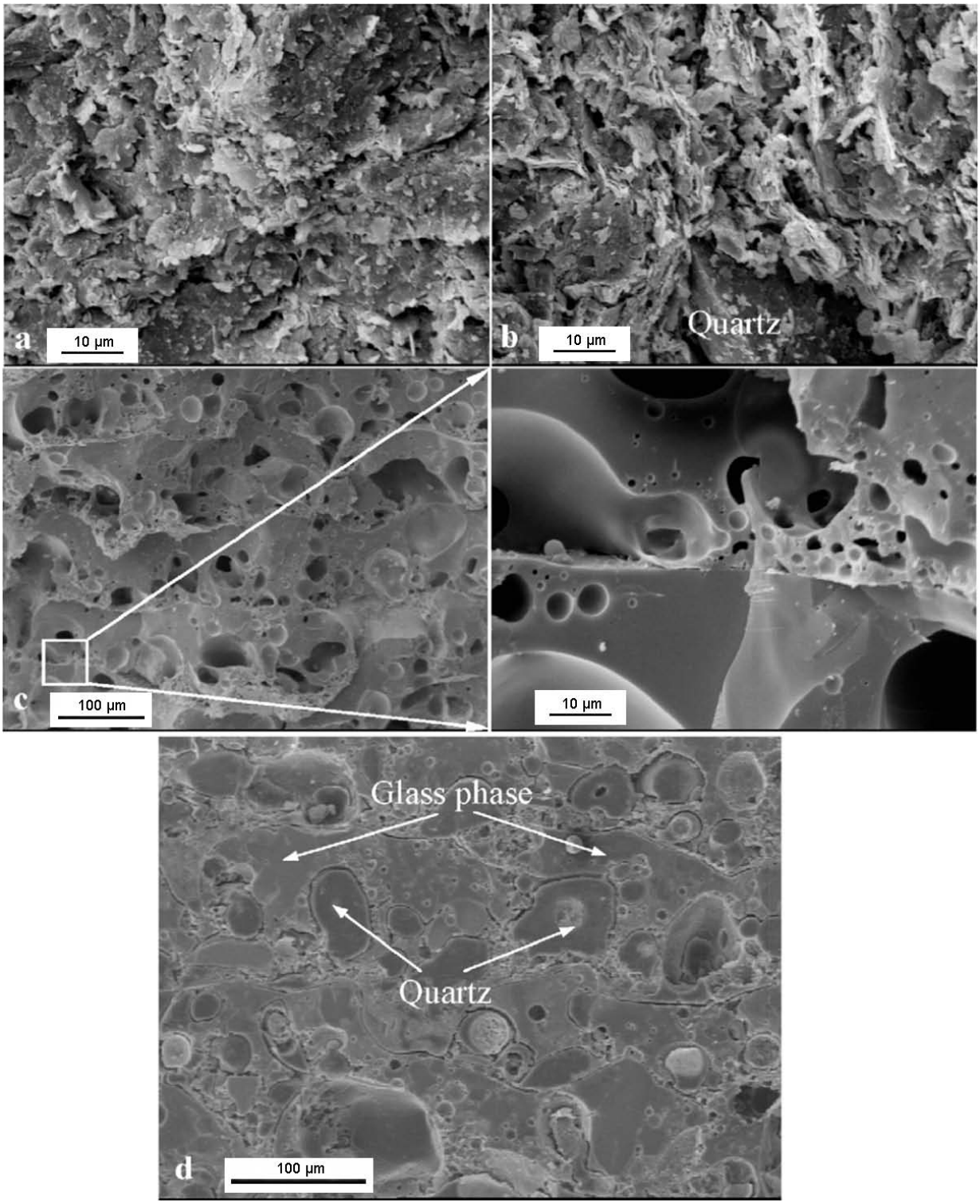

Fig. 2 Cross-sections of the different porcelain samples: (a) dried green body; (b) biscuit-fired body after firing in a furnace at 900 °C; (c) layer-wise laser-sintered with laser power of 20 W, scan speed of 100 mm/s, and hatch spacing of 0.1 mm; (d) polished and etched (10 % HF, 60 s) laser-sintered sample using the same parameters with c (SEM, fracture and polished surface).

Porcelain has a complex chemical composition. The phase transformations are also complex during the laser sintering process, such as dehydroxylation of hydroxyl groups in kaolinite. Dehydroxylation of hydroxyl groups releases H_2O, as shown by the TG/DT analysis results in Fig. 3. It has been proved that pore formation is strongly dependent on the laser beam energy density, but the determining factors are the original porosity and pore size distribution in the matrix [20]. In the present research, the porosity and pore size distribution of the matrix produced by using the layer-wise slurry deposition process could not be changed. However, hatch spacing and laser energy density, which involves the laser power, scan speed, and beam diameter, could be manipulated to tailor the microstructures and control the mechanical strength of the final porcelain components [21].

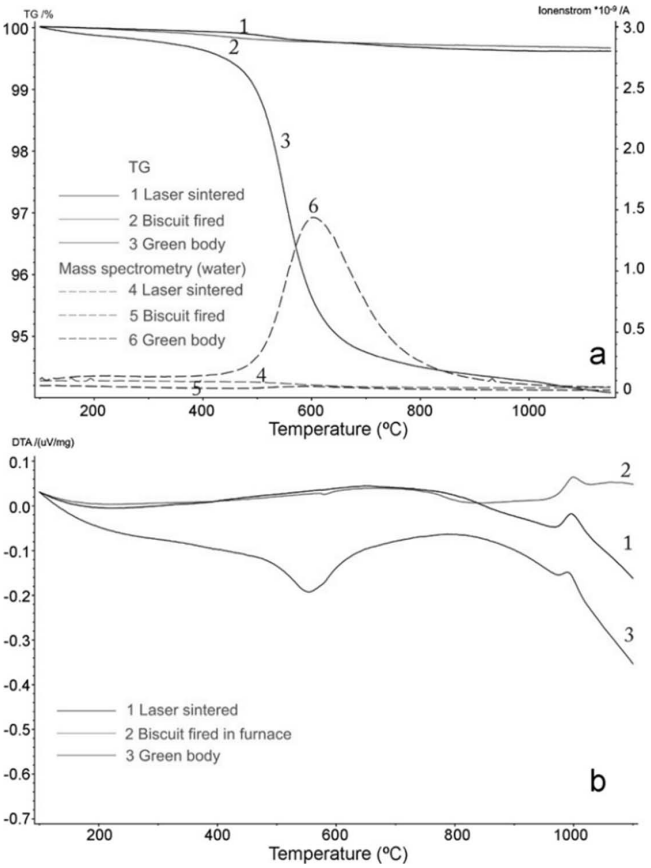

Fig. 3 TG and DT analysis results of three different samples: (1) laser-sintered; (2) furnace pre-sintered and (3) green body.

(b) *TG and DTA*

TG and DT analyses were conducted on the LS, BF samples as well as the porcelain green body. All the results are shown in Fig. 3a. The TG curves for the LS and BF samples are similar in comparison with the green body which has 5 % mass loss at ~ 550 °C (dehydroxylation of kaolinite). The temperature of laser sintering and furnace biscuit firing (900 °C) are all higher than the dehydroxylation temperature range and no residual hydroxyl groups are left in the LS and BF samples. An endothermic peak was found at ~ 550 – 600 °C in the DTA results of the green body (Fig. 3b), probably due to the dehydroxylation of kaolinite and α-to β-quartz phase inversion. The phase inversion of quartz also happens in the furnace-biscuit-fired samples owing to a slight endothermic peak without mass loss being observed. However, there is no peak of α-to β-quartz phase inversion at this temperature for the laser-sintered sample probably because the rapid cooling rate of laser sintering process prevented the reversible transformation of quartz. All the curves have exothermic peaks owing to the spinel crystallization or the formation of mullite around 1000 °C.

(c) *Phase composition*

XRD spectra taken from green bodies reveal the typical triaxial porcelain composition (Fig. 4a). Quartz, kaolinite, and soda feldspar are the major phases. Illite has been also detected in the raw material as a minor phase. Samples biscuit-fired at 900 °C consist of quartz as the only major phase. As mentioned before, a porous, plate-like metakaolin phase is observed in the microstructure, but no metakaolin is detected by means of XRD (Fig. 4b). Metakaolin gives practically no distinct X-ray pattern and was described as an amorphous phase or solid solution before Brindley and Nakahira first proposed a crystal structure (BN model) on the basis of single crystal XRD studies [16]. However, the loss of c-axial periodicity in the metakaolin caused the diffuse XRD pattern (Fig. 4b). Quartz and amorphous phases dominate the XRD spectra taken from laser-sintered samples (Fig. 4c), which is consistent with the microstructural observations (Fig. 2c). The quartz from the starting composition (raw material) has not been completely dissolved into the surrounding amorphous phase owing to the short laser-material interaction time. No mullite phase was found in the XRD analysis of the LS sample (Fig. 4c). Mullite phase was not observed in the polished and etched cross-sections of LS sample either (Fig. 2d). Apparently, the formation of significant amounts of mullite phase takes some time. On the other hand, mullite phase was observed in the laser-sintered SiO_2-Al_2O_3 system [12]. The likeliest explanation of the lack of mullite in this laser-sintered porcelain system is that the concentration of Al_2O_3 did not reach the critical value for mullite nucleation [22, 23].

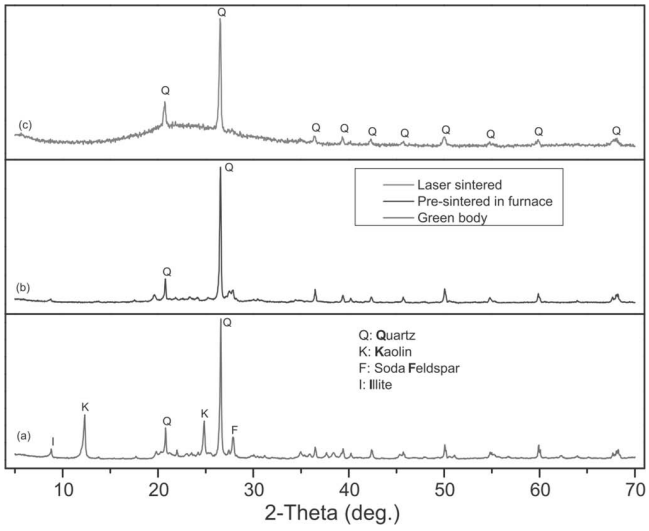

Fig. 4 XRD analysis results of different porcelain samples.

(d) ***Density***

The density and porosity measurement results are shown in Fig. 5. BF samples have a slightly higher density (true, bulk, and apparent) than the LS ones. Contributions from glassy phases probably cause the relatively low true density of the LS samples. Metakaolin is the dominant phase in BF samples. Metakaolin has a maximum density of 2.64 g/cm^3 at 900 °C before decomposition in a spinel-type phase [17]. This could be the reason why the density of BF samples is higher than that of LS samples. The total porosity of the two types of samples is comparable, 27.4 % and 30.6 %, respectively; even though the laser-sintered samples have a much larger average pore radius than the furnace-sintered samples.

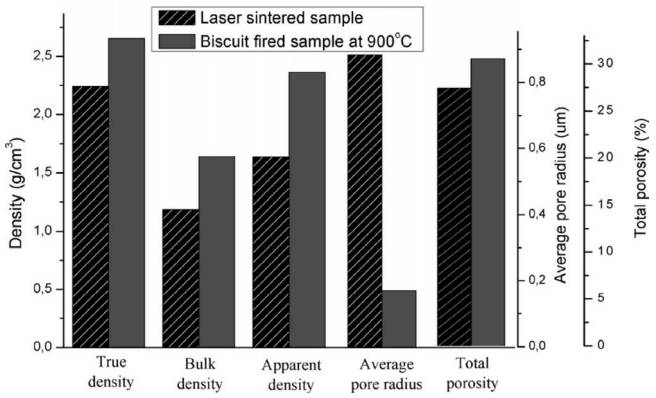

Fig. 5 Results of the mercury intrusion measurement.

(2) Post-Sintered Samples

(a) ***Shrinkage in the post-sintering process***

The shrinkage curves of the LS and BF samples were measured with a dilatometer (up to 1500 °C). The maximum shrinkage rate of BF samples is observed at 1380 °C, as shown in Figs. 6 and 7. The rate of shrinkage is reduced at temperatures over 1380 °C, which is probably caused by the expansion of trapped gas in the ceramic body. The shrinkage curve for the BF sample in Fig. 6 reflects the typical sintering behavior of porcelain bodies [24, 25, 26]. Laser-sintered samples have been studied with two different scan patterns, as shown by the insets in Fig. 6. In scan pattern A the scan vectors are parallel to the axis of the shrinkage measurement direction whereas the scan vectors in scan pattern B are perpendicular to this axis. The different shrinkage curves of the two scan patterns reflect the anisotropy of laser-sintered bodies in different directions. The directionality of the laser sintering process caused the different morphology of the microstructure in different directions and consequently the diverse shrinkage in different directions [13]. The length of the laser scan vectors also affects the real temperature in the heat-affected zone even with the same laser sintering parameters [26]. Difference in the sintering temperature also induces different microstructures as well as the shrinkage. These intrinsic differences in the shrinkage in three directions are inevitable and can only be compensated by adjusting the three-dimensional scale factors before the fabrication process starts. The shrinkage rates derived from the shrinkage curves are shown in Fig. 7. There are two peaks for each curve. The first peak at around 980 °C was probably caused by the transformation of metakaolin to spinel-type phase [17] and the formation of a eutectic liquid phase between amorphous silica and soda feldspar [15]. The second peak for the furnace biscuit-fired sample at 1150 °C could be considered as the formation of mullite and further liquid phase. The shrinkage rates can be used to determine the post-sintering schedule by setting a low heating rate in the range of high shrinkage to avoid delamination or crack formation in the laser-sintered ceramic bodies. Photos taken of the samples after dilatometer measurement are shown in Fig. 8. All the samples turned black during the measurement probably as a result of the nitrogen atmosphere in the dilatometer furnace. No cracks or delamination were observed in the biscuit-fired sample (Fig. 8c). However, obvious delamination appeared in the laser-sintered samples, especially in the sample with scan pattern B. In the present research, laser-sintered samples were also post-sintered in a conventional furnace at 1380°C with air atmosphere and no obvious delamination was observed in these samples (Fig. 10a). So, it is still unclear if the delamination was caused by the nitrogen atmosphere or the high sintering temperature (1500 °C) in the dilatometer measurement.

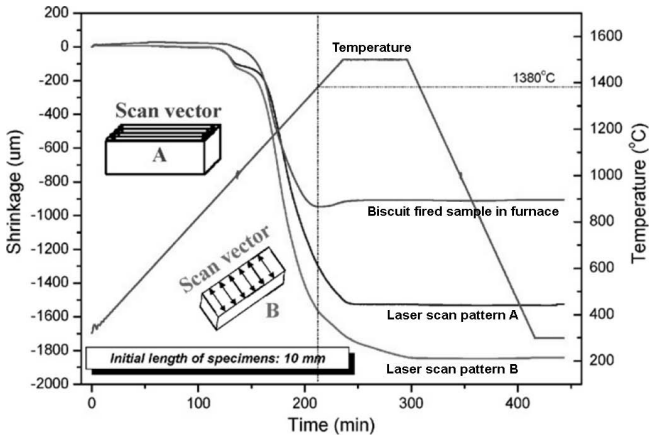

Fig. 6 Shrinkage curves from the dilatometer measurement.

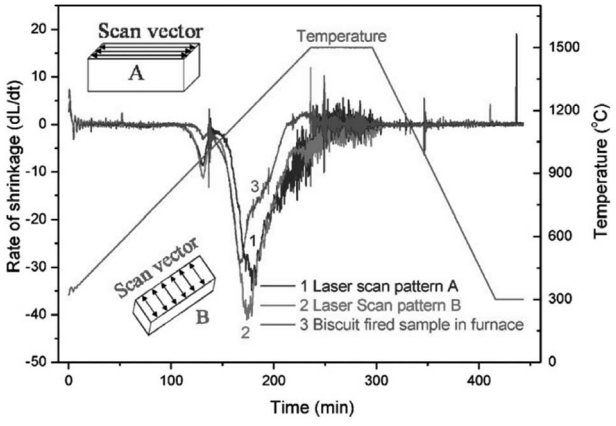

Fig. 7 Shrinkage rate curves derived from the shrinkage curves.

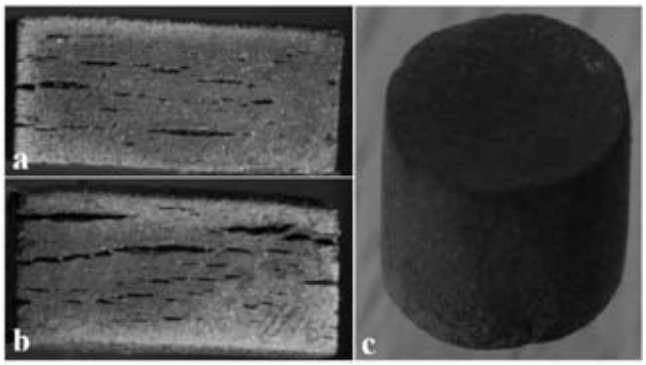

Fig. 8 Samples after the dilatometer measurements: (a) scan pattern A, (b) scan pattern B, (c) furnace biscuit-fired sample (digital photos).

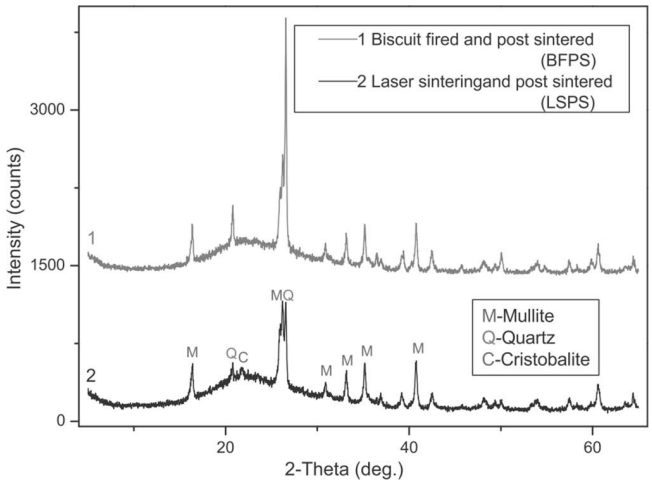

Fig. 9 XRD results of the samples after being post-sintered in a furnace at 1380 °C for 1 h.

(b) ***Phase composition and microstructure***

XRD patterns of laser-sintered and biscuit-fired samples after post-sintering in the furnace are shown in Fig. 9, namely LS post-sintered (LSPS) and BF post-sintered (BFPS) samples respectively. Mullite, quartz, and amorphous phases were detected in the BFPS sample. In comparison with the BFPS samples, the LSPS samples show a relatively high intensity of mullite phase, while cristobalite was also found in this sample. The high content of mullite phase in the LSPS samples probably originates from an abundant amorphous phase in the laser-sintered samples, as shown in Figs. 2c and 4c. Abundant liquid amorphous phase provided a more active initial condition for the transformation of mullite phase than that in the BF sample when post-sintered in the furnace. The formation of cristobalite only in the LSPS porcelain sample is also induced by the abundant liquid phase in the laser-sintered bodies because the cristobalite may form as a devitrification product from the glass phase when the melting phase becomes saturated with silica [27]. The micrographs of fractured and etched cross-sections of post-sintered samples are shown in Fig. 10. There is no delamination observed in the LSPS sample, as shown in Fig. 10a. The post-sintering removes the distinct boundaries between adjacent layers. A porous microstructure with a porosity of 13.4 % for the LSPS bodies has been obtained. Most of the pores are homogenously distributed around the interfaces between two adjacent layers, which are indicated by the lines between two layers in Fig. 10a. In the BFPS sample, unidirectional elongated bubbles are observed in Fig. 10c. The size of the unidirectional elongated bubbles is almost 200 μm, which is much bigger than the round pores in the matrix. These unidirectional elongated bubbles were formed by pore coalescence in which small pores collide with big ones owing to the velocity difference of the pores in the liquid phase during the post-sintering process. The direction of the elongated bubbles was probably influenced by the slip casting process used to produce this sample. The plate-like kaolinite particles and unidirectional absorption of water from the inside of the part to the plaster moulds probably caused this heterogeneous microstructure with unidirectional elongated bubbles. Furnace-post-sintered samples are basically constituted by mullite, quartz, and glass phases, as shown in Figs. 10b and d. In the LSPS sample (Fig. 10b) residual quartz particles are surrounded by the silica saturated glass phase, which is the matrix and source for the transformation of cristobalite phase by devitrification of the glass phase. In comparison with the LSPS sample there is no silica saturated glass phase obtained in the microstructure (Fig. 10d).

(c) ***Properties of the final ceramic components***

The properties of the final ceramic components are listed in Table 1. BF post-sintered (BFPS) ceramic samples have a much higher bending strength than LS post-sintered (LSPS) samples even though the total porosity of the two samples is similar. Surface polishing could improve the mechanical strength of both samples. The low bending strength of laser- and post-sintered LSPS sample is probably caused by the relative low bulk density, which has a critical influence on the mechanical strength. Laser parameters also have a significant influence on the mechanical properties and should be optimized in future work in order to approach the properties of traditional porcelain. The BF samples were just cut from the biscuit-fired porcelain blocks and the LS samples were prepared by means of laser sintering. Surface polishing could probably improve the mechanical strength to some extent. But for the LSPS samples newly produced surface defects will appear during the surface polishing process owing to the layered and porous microstructure. So, the surfaces of all the samples were not polished before the bending tests.

The shrinkage of LS samples during post sintering was measured. Shrinkage in the length direction (6.58 ± 0.14 %), which is consistent with the laser scanning vectors, has a relative small value and is comparable with that of the BF sample. But shrinkage in the height and width directions, which are the layer deposition and hatch spacing directions respectively, are much larger than that in the length direction as most of the pore coalescence happens in these two directions instead of in the length direction (direction of laser scanning vectors). The shrinkage in the other two directions for the BF sample might be different owing to the unidirectional elongated bubbles but was not measured in the present research.

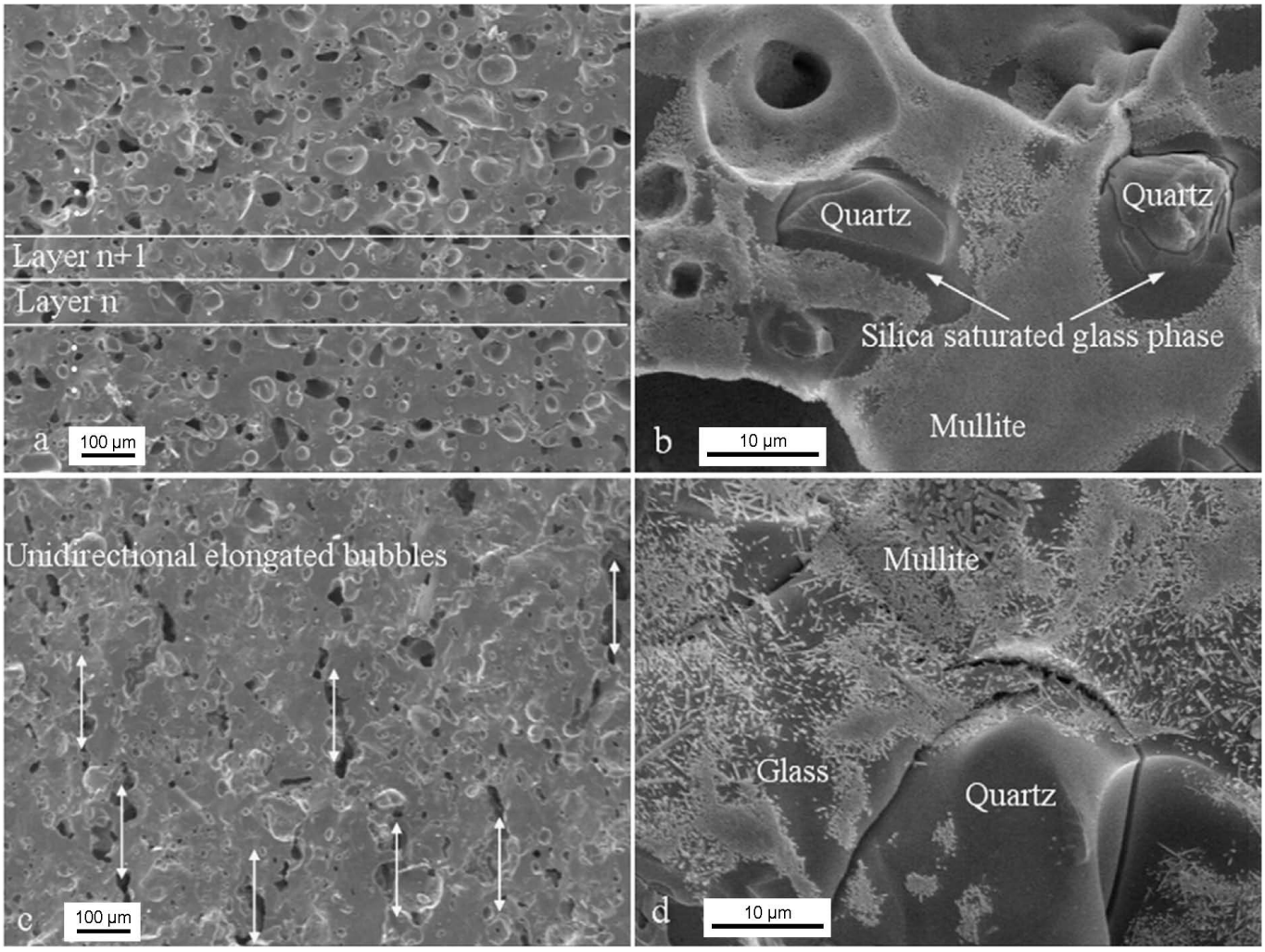

Fig. 10 Micrographs of the samples post-sintered in the furnace at 1380 °C for 1 h: (a) fractured and (b) etched (10 % HF, 60 s) cross-section of laser-sintered sample; (c) and (d) of furnace biscuit samples, respectively (SEM, fracture surfaces).

Table 1: Properties of furnace post sintered porcelain samples prepared by laser sintering and conventional biscuit firing processes (at 1380 °C for 1 h).

	Bending strength (MPa)	True density (g/cm^3)	Bulk density (g/cm^3)	Apparent density (g/cm^3)	Total porosity (%)	Shrinkage (%)		
						Length	Height	Width
LSPS	25.9 ± 3.0	2.14 ± 0.02	1.77 ± 0.07	2.04 ± 0.08	13.40 ± 0.32	6.58 ± 0.14	9.11 ± 0.83	9.17 ± 0.18
BFPS	48.9 ± 0.9	2.28 ± 0.02	1.92 ± 0.03	2.28 ± 0.05	13.08 ± 0.24	6.35 ± 0.33	N/A	

(3) Potential Applications

A thick wall pipe was successfully fabricated with the LSD process in order to demonstrate the feasibility of rapid prototyping for voluminous parts, such as sanitaryware; Fig. 11. This model has a height of 94 mm, an outer diameter of 61 mm and a wall thickness of 6 mm. In order to show the ability of the LSD process to generate delicate structures, a structure was attached to the outer surface of the pipe. The minimum feature size of this structure is 0.1 mm. Another model produced in present research is the double heart, as shown in Fig. 12. Geometries like this could not be produced with the conventional fabrication process. Thanks to our LSD process, users can design any geometry and fabricate it in the machine

without any special tools. Also no support structure during build-up of the models is required, as the powder bed itself is rigid enough for fixing the models. A glazed and glost-fired double heart is presented in Fig. 12b. The surface quality, which is the primary consideration for artwork, is comparable with the parts produced with traditional methods. It has proven that the porcelain products (e.g. whitewares and artworks) can be produced with this rapid prototyping process in a relatively short time.

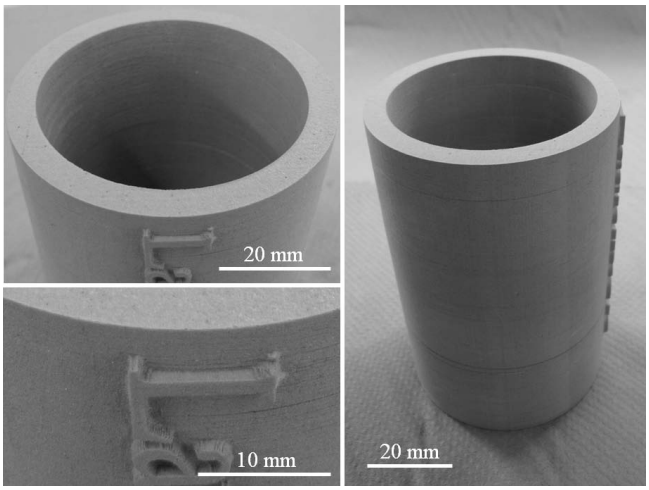

Fig. 11 Voluminous prototype: height 94 mm, outer diameter 61 mm and wall thickness 6 mm. This prototype is to show that voluminous parts with a wall thickness comparable to sanitaryware can be manufactured with the LSD process. As the prototype has not been manufactured in a consecutive run, but in five shifts, slight irregularities are noticeable, each approximately 19 mm in height.

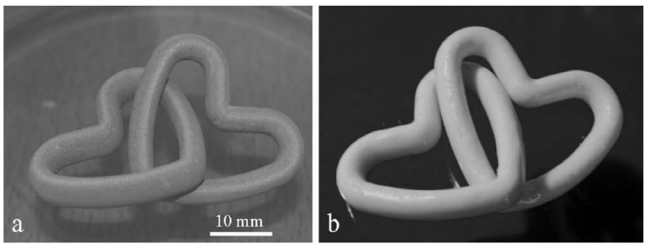

Fig. 12 Porcelain double hearts produced by rapid prototyping: (a) laser-sintered and then (b) glazed and glost-fired (digital photos).

IV. Conclusions

The feasibility of rapid prototyping of porcelain products has been validated by the studies on the properties of laser-sintered (LS) and biscuit-fired (BF) samples. After post-sintering (PS), the final ceramic samples have similar porosity of about 13 %. The bulk density of the LSPS samples was 0.15 g/cm^3 and thus lower than that of the BF-PS samples. The mechanical strength of the former (25.9 ± 3.0 MPa) was much lower than that of the latter (48.9 ± 0.9 MPa). However, the mechanical strength has been verified as sufficient for treatment such as glazing and glost firing. The possibility of rapid prototyping of porcelain components has been demonstrated with two models, a voluminous thick-wall pipe and a double heart, produced with the LSD process.

References

1 Jacobs, F.P.: Rapid prototyping and manufacturing fundamentals of stereolithography, Dearborn, SME, (1992).

2 Nelson, J.C., Xue, S., Barlow, J.W., Beaman, J.J., Marcus, H.L., Bourell, D.L.: Model of the selective laser sintering of bisphenol-a polycarbonate. *Ind. Eng. Chem. Res.,* **32**, 2305 – 17, (1993).

3 Yardimci, M.A., Guceri, S.: Conceptual framework for the thermal process modeling of fused deposition, *J. Rapid Prototyp.*, **2**, 26 – 30, (1996).

4 Das, S., Wohlert, M., Beam, J.J., Bourell, D.L.: Producing metal parts with selective laser sintering/hot isostatic pressing, *JOM*, **50**, 17 – 20, (1998).

5 Mazumder, J., Choi, J., Nagarthnam, K., Koch, J., Hetzner, D.: The direct metal deposition of H13 tool steel for 3D components. *JOM,* **49**, 55 – 60, (1997).

6 Griffith, M.L., Halloran, J.W.: Freeform fabrication of ceramics via stereolithography, *J. Am. Ceram. Soc.*, **79**, 2601 – 8, (1996).

7 Allahverdi, M., Danforth, S.C., Jafari, M., Safari, A.: Processing of advanced electroceramic components by fused deposition technique, *J. Eur. Ceram. Soc.*, **21**, 1485 – 90, (2001).

8 Grida, I., Evans, J.R.G.: Extrusion freeforming of ceramics through fine nozzles, *J. Eur. Ceram. Soc.*, **23**, 629 – 35, (2003).

9 Bertrand, P.H., Bayle, F., Combe, C., Goeuriot, P., Smurov, I.: Ceramic components manufacturing by selective laser sintering, *Appl. Surf. Sci.*, **254**, 898 – 992, (2007).

10 Regenfuss, P., Streek, A., Ullmann, F., Kuehn, C., Hartwig, L., Horn, M., Exner, H.: Laser micro sintering of ceramic materials: part 2. *Interceramics*, **57**, 6 – 9, (2008).

11 Günster, J., Engler, S., Heinrich, J.G.: Forming of complex-shaped ceramic products via layer-wise slurry deposition (LSD), *Bull. Eur.Ceram.Soc.*, **1**, 25 – 8 (2003).

12 Gahler, A., Heinrich, J.G., Günster, J.: Direct Laser Sintering of Al_2O_3-SiO_2 Dental ceramic components by layer-wise slurry deposition, *J. Am. Ceram. Soc.*, **89**, 3076 – 80, (2006).

13 Tian, X., Günster, J., Melcher, J., Li, D., Heinrich, J.G.: Process parameters analysis of direct laser sintering and post treatment of porcelain components using taguchi's method, *J. Eur. Ceram. Soc.,* **29**, 1903 – 15, (2009).

14 Kingery, W.D.: Introduction to ceramics. New York, London: John Wiley &Sons, Inc., (1960).

15 Carty M.W., Senapati U.: Porcelain — raw materials, processing, phase evolution, and mechanical behavior, *J. Am. Ceram. Soc.*, **81**, 3 – 20, (1998).

16 Nakahira, M., Brindley, W.G.: The kaolinite-mullite reaction series: I. A survey of outstanding problems, *J. Am. Ceram. Soc.*, **42**, 311 – 4, (1959).

17 Nakahira, M., Brindley, W.G.: The kaolinite-mullite reaction series: II Metakaolin, *J. Am. Ceram. Soc.*, **42**, 314 – 8, (1959).

18 Roy, R., Roy, D.M., Francis, E.E.: New data on thermal decomposition of kaolinite and halloysite, *J. Am. Ceram. Soc.*, **38**, 198 – 205 (1995).

19 Brindley, G.W., Hunter, K.: Thermal reactions of nacrite and the formation of metakaolin, alumina and mullite, *Miner. Mag.*, **228**, 574 – 84, (1955).

20 Triantafyllidis, D., Li, L., Stott, F.H.: Mechanisms of porosity formation along the solid/liquid interface during laser melting of ceramic, *Appl. Surf. Sci*, **208 – 209**, 458 – 62, (2003).

21 Tian, X., Sun, B., Heinrich, J., Li, D.: Stress relief mechanism in layer-wise laser directly sintered porcelain ceramics, *Mater. Sci. Eng. A*, **527**, 1695 – 703, (2010).

22 Heinrich, J.G., Gahler, A., Günster, J., Schmuecker, M., Zhang, D., Zhang, J., et al.: Microstructural evolution during direct laser sintering in the Al_2O_3-SiO_2 system, *J. Mater. Sci.*, **42**, 5307 – 11, (2007).

[23] Schmuecker, M., In: Schneider H, Komarneni S, (editors): Mullite, Weinheim, Wiley VCH, (2005).

[24] Isik, E.O., Nakagawa, Z.: Bending strength of porcelains, *Ceram. Int.*, **28**, 131 – 40, (2002).

[25] Maity, S., Sarkar, B.K.: Development of high-strength whiteware bodies, *J. Eur. Ceram. Soc.,* **16**, 1083 – 8, (1996).

[26] Tian, X., Sun, B., Heinrich, J.G.: Scan pattern, stress and mechanical strength of laser directly sintered ceramics, submitted.

[27] Schneider, H., Majdic, A., Vasudevan, R.: Kinetics of the quartz-cristobalite transformation in refractory-grade silica materials, *Mater. Sci. Forum*, **7**, 91 – 102, (1986).